# Predicting "Springback" Using 3D Surface Representation Techniques: A Case Study in Sheet Metal Forming

S. El Salhi, F. Coenen, C. Dixon, M. S. Khan

*University of Liverpool, Department of Computer Science, Ashton Building, Ashton Street, Liverpool L693BX, United Kingdom.*

## Abstract

Three different mechanisms are presented to allow for the representation of 3D surfaces in such a way that key features are retained while at the same time ensuring compatibility with prediction (classification) techniques. The application domain is sheet metal forming. The representations are designed to capture the nature of the surface to be manufactured and predict deformations, known as "springback", that will occur across a surface (in a non-uniform manner) as a result of the application of a sheet steel forming process. The three representation techniques are: (i) Local Geometry Matrices (LGMs) founded on the concept of local binary patterns, (ii) Local Distance Measure (LDM) founded on the observation that the springback magnitude is affected by distance from edges and (iii) Point Series (PS) whereby local geometries are represented in terms of a linearisation. The evaluation of each of the techniques, and variations thereof, using parts that have been manufactured especially for the purpose, is fully described. The paper also reports on a statistical significance test concerning the results.

*Keywords:* 3D surface representation, Classification, Springback prediction

## 1. Introduction

The phenomena of *springback* is a significant issue with respect to the sheet metal forming industry (Cafuta et al., 2012; Jeswiet et al., 2005). Springback is the deformation introduced into some manufactured part as a result of applying some forming process. As a consequence the desired shape, some prescribed 3D surface ($T$), is not the same as the generated surface ($T'$), hence the quality of the manufactured part is compromised. The nature (magnitude and direction) of springback is related to the local geometries describing the 3D surface to be manufactured. If we can predict springback we can apply correcting measures to $T$ to produce $T''$ so that the generated surface $T'$ will approximate much more closely to $T$. Thus given a previously manufactured part, with known springback, we wish to produce a classifier that can predict springback with respect to a particular manufacturing process (such as Asymmetric Incremental Sheet Forming or AISF). The challenge is how best to represent the 3D surfaces of interest so as to facilitate the effective capture of local geometries to which individual springback dimensions can be related. The work presented in this paper is directed at exploring a number of alternative techniques for capturing the nature of 3D surfaces so as to support the effective generation of springback predictors (classifiers).

Three different 3D surface representation techniques are proposed: (i) Local Geometry Matrix (LGM), (ii) Local Distance Measure (LDM) and (iii) Point Series (PS). The LGM representation is founded on the idea of Local Binary Patterns (LBPs) as described in (Guo et al., 2010). The LDM representation is motivated by the observation that the local magnitude of springback tends to increase with the distance from edges. The PS representation is based on the idea

*Email addresses:* hsselsal@liverpool.ac.uk (S. El Salhi), coenen@liverpool.ac.uk (F. Coenen), cldixon@liverpool.ac.uk (C. Dixon), mskhan@liverpool.ac.uk (M. S. Khan)

of representing local geometries in terms of a point series curve (linearisation).

The main contributions of this paper are as follows.

1. A generic framework for springback prediction.

2. The LGM technique to represent 3D surfaces in terms of *local geometries*.

3. The LDM technique to represent 3D surfaces local geometries in terms of *distances* to the nearest critical features (edges or corners).

4. The PS technique to represent 3D surfaces local geometries in terms of linearisations of points to form point series (curves).

5. Extensive comparison of the three proposed techniques in terms of accuracy and AUC measurements.

6. A statistical evaluation to identify the significant difference in operation between the use of LGM, LDM and PS in the context of 3D surface classification.

The operation of the three proposed techniques are compared in this paper using two flat-topped pyramid surfaces (shapes) which were specially manufactured with respect to the work described (hence the degree of springback is known).

The rest of this paper is organised as follows. Section 2 presents a literature review of related work to that presented in the rest of this paper. Section 3 starts by introducing a generic framework for springback prediction. The three different representation techniques (LGM, LDM and PS) are then described in Sections 4, 5 and 6 respectively. The evaluation of the proposed representations, in the context of classifier generation, using the two flat topped pyramid shapes is presented in Section 7. Some conclusions are presented in Section 8.

## 2. Related Work

In the field of 3D representation many different techniques have been proposed directed at a variety of goals and objectives in the context of a range of application domains. Example applications include: (i) the translation of physical 3D surfaces into Computer Aided Graphics (CAG) formats (Hsiao & Chen, 2013; Jahanshahi & Masri, 2012), and (ii) rendering in the context of computer vision (Ayache, 1995; Izquierdo & Ohm, 2000) and with respect to many medical image analysis domains (Ayache, 1995; Ghanei et al., 1998; Fresno et al., 2009). Existing 3D representation techniques can be categorised according to the objective associated with the representation. High level examples of such 3D object representation techniques include:

- **Point Clouds**: The simplest representation is a point cloud representation whereby a 3D surface is defined in terms of an unordered collection of points defined in terms of x, y, and z coordinates typically generated using either CAD software or some optical measuring tool (Alexa et al., 2001; Hoppe et al., 1992; Roth & Wibowoo, 1997).

- **Range Images**: Range images are 2D images depicting the distance of points in a 3D environment from a specific point, normally associated with some type of sensor device (Soucy & Laurendeau, 1995).

- **Surface Representation**: For 3D surface representation commonly advocated techniques include: (i) mathematical techniques (implicit and parametric) (Farin et al., 2002; Munkberg et al., 2010) and (ii) mesh representations (Adams, 2013).

- **Volume Representations**: For volumetric data the idea of Constructive Solid Geometries (CSG) can be adopted whereby a hierarchy of boolean operations (union, difference and intersection) are applied to a collection of basic volumes so as to define more complex 3D volumes (Goldfeather et al., 1986).

- **High-level Representations**: For high-level representations graphs are frequently used, examples include: (i) Reeb graphs (Biasotti et al., 2008), (ii) scene graphs (Song & Yang, 2011) and (ii) "skeletons" (Demoly et al., 2011).
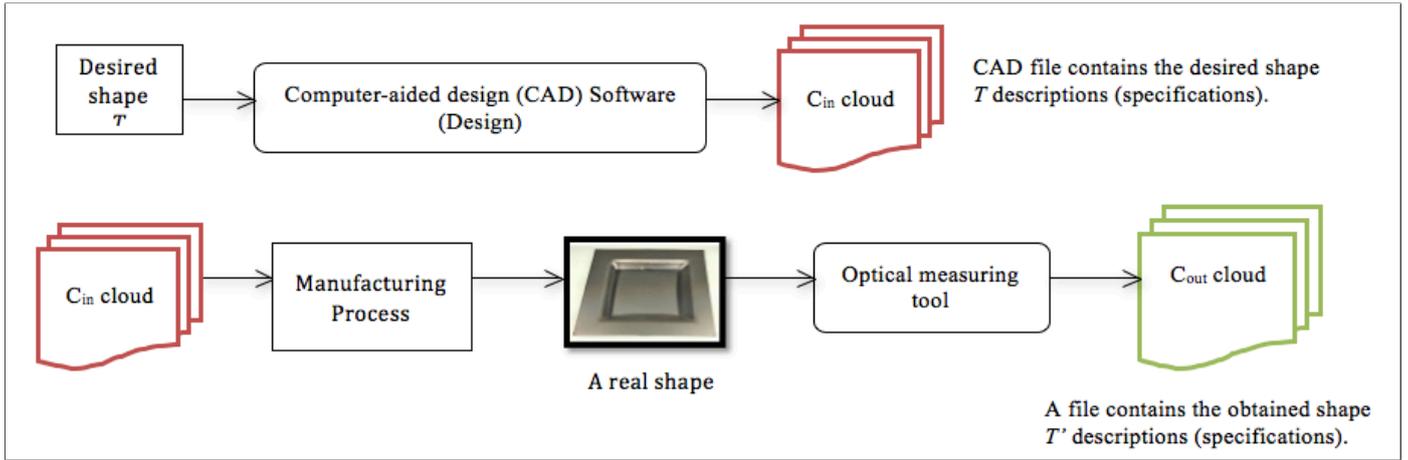
Figure 1: The process for obtaining the $C_{in}$ and $C_{out}$ 3D surface specifications.

For a more detailed discussion concerning 3D representation techniques interested readers are referred to (Hubeli & Gross, 2000) where the authors present a taxonomy of various 3D representation techniques.

Classification (prediction) is the branch of machine learning (knowledge discovery in data) concerned with the automated generation of software systems that can be used to label previously unseen data. Classification is a supervised learning technique in the sense that it requires pre-labelled data to be used to "train" the desired classifier. Many different classifier generation techniques have been proposed, to date no single general-purpose "best" technique has been identified. Two particular techniques have been used with respect to the work described in this paper: (i) Decision Trees (Breiman et al., 1984; Quinlan, 1986, 1993) and (ii) k-Nearest Neighbour (k-NN) (Dasarathy, 1991; Wettschereck, 1994). Decision trees were selected because: (i) they are one of the top ten most popularly used classification techniques (Wu et al., 2007), (ii) they are easily interpreted, and (iii) it is straight forward to extract rules from the generated trees (rules that can be used to furnish explanations). In addition, in previous work published by the authors (El-Salhi et al., 2012; Khan et al., 2012) it has been shown that in the context of 3D representations for springback prediction there is no significant differences in operation between decision trees and other popular classification techniques (Naïve Bayes and classification association rule generators such as CMAR, CPAR and TFPC). However, the use of decision trees was only appropriate with respect to the LGM and LDM representations which leant themselves to the use of a feature vectors. For the PS representation the local geometries contained within a given 3D surface are represented in terms of individual point series (linerisations) and hence a k-NN technique was used to label new curves (curve matching was conducted using Dynamic Time Warping).

Dynamic Time Warping (DTW) is a well established technique originally used to define the similarity between two time series, although it is equally applicable to point series. It was first proposed in (Sakoe & Chiba, 1990) in the context of speech recognition. DTW has since been applied with respect to a wide range of applications (Keogh & Pazzani, 2001; Wei & Keogh, 2006). Given two point series $A$ and $B$ of length $n_a$ and $n_b$ respectively, such that $n_a$ does not necessarily equal $n_b$, DTW is used to produce a distance measure describing the similarity between the two curves regardless of the individual lengths of $A$ and $B$.

Sheet metal forming is a widely used process with respect to manufacturing industries such as the aircraft and automotive industries. One such process is Asymmetric Incremental Sheet Forming (AISF) where a tool head follows a predefined tool path to "push out" a desired shape (Jeswiet et al., 2005). The main advantages of AISF, over alternative sheet metal forming processes, are reduced time and cost (Strano, 2005). However, the main limitation of the AISF process is the significant amount of springback that results. As already noted above, springback is the

elastic deformation that occurs as a result of the application of a sheet metal forming process. Generally speaking springback is related to both manufacturing parameters (the 3D geometry of the shape to be manufactured) and material properties (Firat et al., 2008; Nasrollahi & Arezoo, 2012; Liu et al., 2008). There has been substantial reported work on springback characterisation and analysis. Of note are the Finite Element Method (FEM) and Artificial Intelligent methods that have been proposed to predict springback (Chatti & Hermi, 2011; Narasimhan & Lovell, 1999; Yoon et al., 2002). Although FEM provides a flexible simulation environment (parameters can be easily modified), FEM is a time consuming option (Hao & Duncan, 2011; Tisza, 2004; Firat et al., 2008). Furthermore, FEM has been found to be not as accurate as originally expected because of the use of simplification assumptions with respect to the required integration calculation (Chatti, 2010; Chatti & Hermi, 2011; Nasrollahi & Arezoo, 2012). Artificial Neural Network (ANNs) are often quoted as being a good alternative to FEM. However, the computational resource requirement is a significant limitation to the use of ANNs in the context of springback characterisation (Liu et al., 2007; Fu et al., 2010). To the best knowledge of the authors there has been no reported work on the application of classification techniques (or data mining techniques in general) for the purpose of predicting springback in the context of AISF in particular, and sheet metal forming in general.

## 3. Springback Prediction Framework

This section presents the general Springback Prediction Framework developed by the authors. The three proposed 3D surface representation techniques are presented in the following three sections, Sections 4, 5 and 6. The framework encompasses both the generation of the desired classifier and its usage. Note that the first requires a training set. To generate a training set the framework requires input of two point clouds $C_{in}$ and $C_{out}$ associated with some 3D surface $T$ obtained as shown in Figure 2. The $C_{in}$ cloud describes the desired surface (design specification) typically obtained using some form of Computer-Aided Design (CAD) Software. The $C_{out}$

cloud describes the surface that was actually manufactured ($T'$) and is typically obtained by using some form of optical measuring tool[1].

The points in both the $C_{in}$ and $C_{out}$ clouds are defined in terms of a x, y and z coordinate system and are translated into two 2D grids, $G_{in}$ and $G_{out}$ respectively, of grid size $d$. Each grid square is referenced by its centre point defined in terms of a x and y coordinate pair with an associated z-value (the average of the z coordinate for all the points located within the grid square). The main advantages for the grid representation are: (i) it minimise the density of the point clouds, (ii) it minimise the computation time required to process the point clouds, (iii) it permits straightforward further processing, (iv) it provides for an integrated and unified framework for both $C_{in}$ and $C_{out}$, (v) it provide a simple referencing system between corresponding grid squares in $C_{in}$ and $C_{out}$ and (vi) its supports an efficient identification of the local neighbouring grid points (Jain et al., 1995; Lu & Sajjanhar, 1999; Pinto et al., 2012). Note that once a classifier has been generated, the framework only requires a $C_{in}$ cloud.

Examples of a $G_{in}$ and a corresponding $G_{out}$ grid ($d = 1$mm) for a flat topped pyramid shape, made out of sheet steel using the AISF process, are presented in Figure 3 and 4 respectively. By inspecting the figures the differences between $G_{in}$ and $G_{out}$ can be observed, especially with respect to: (i) the degree of concavity on the side walls and (ii) the deformation in the flat area around the edge of the pyramids.

In the case of training set derivation, once $G_{in}$ and $G_{out}$ have been derived the next stage is to determine the degree of springback (the error value $e$) to be associated with each grid square in $G_{in}$. The process for this is as follows, for each grid square in $G_{in}$:

1. Find the normal of the centre grid point $\vec{n}$ using vector products. In this manner four normals can be found from the dot products of pairs of 90° separated vectors connecting the current grid square centre to its north, south, east and west neighbours.

---

[1]The GOM (Gesellschaft für Optische Messtechnik mbH) optical measuring tool was used with respect to the work described in this paper more details of which can be found in (Berger et al., 2011).
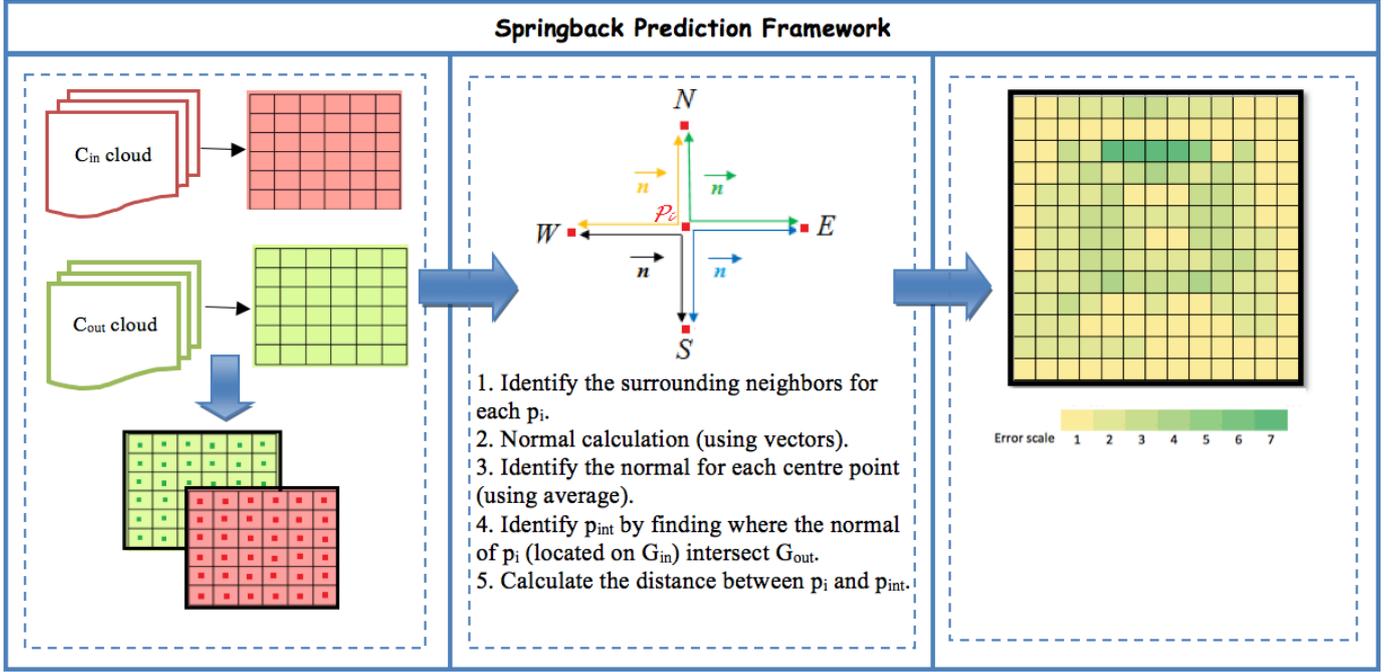
Figure 2: Springback Calculation.
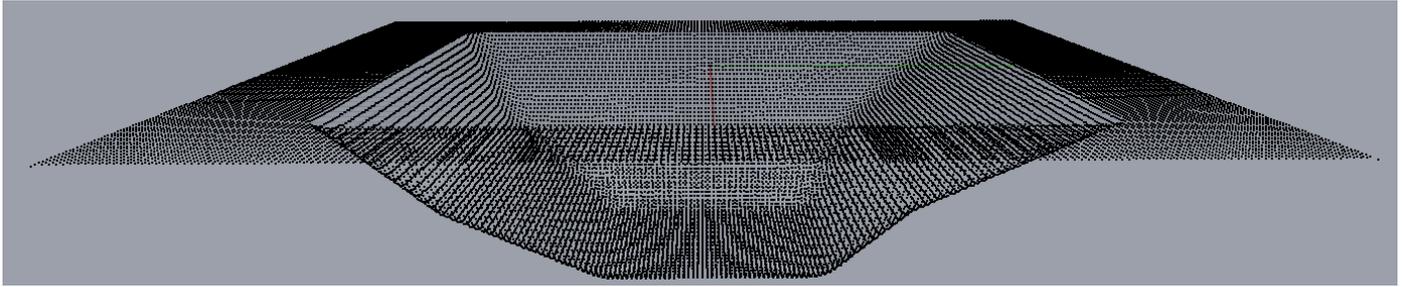


Figure 3: Example $G_{in}$ grid for a flat topped pyramid 3D surface ($d = 1$mm).
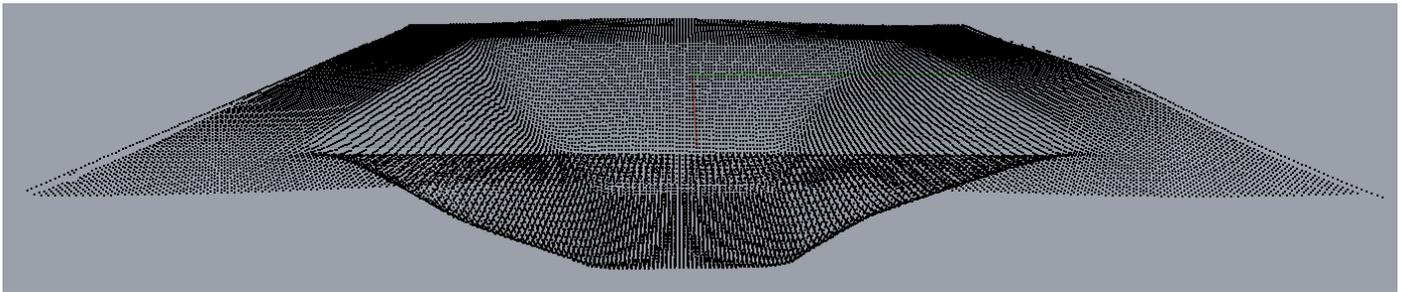


Figure 4: Example $G_{out}$ grid for a flat topped pyramid 3D surface ($d = 1$mm), corresponding to the $G_{in}$ grid given in Figure 3.

2. Identify the intersection point $p_{int}$ located on $G_{out}$ by extending each normal $\vec{n}$ from $G_{in}$ to where they cuts $G_{out}$.

3. Determine the distance along each normal $\vec{n}$

using vector and plane geometry (see Equation 1 where $\vec{n} = \langle a, b, c \rangle$ is the normal originating from a point $p_i(x_i, y_i, z_i)$ located on $G_{in}$ and $p_{int}(x_{int}, y_{int}, z_{int})$ is the corresponding point on $G_{out}$ where the normal intersects $G_{out}$.

4. The average of the four calculated distances then defines the magnitude of the springback error $e_i$ at centre $p_i$, the sign ($+$ or $-$) defines the direction.

The process is illustrated in Figure 2. Referring to the figure we commence with $C_{in}$ and $C_{out}$ point clouds (left hand panel), we the calculate the spring back error for each gird square centre point using vector geometry (middle panel), which is then associated withy each grid square (right hand panel).

$$e_i = \frac{|a(x_i - x_{int}) + b(y_i - y_{int}) + c(z_i - z_{int})|}{\sqrt{(a^2 + b^2 + c^2)}} \quad (1)$$

## 4. Local Geometry Matrix (LGM) Representation

The first 3D surface representation mechanism considered is the Local Geometry Matrix (LGM) mechanism. The concept of LGMs is founded on the idea of Local Binary Patterns (LBPs) as frequently used with respect to image texture analysis. A local geometry matrix is a $n \times n$ grid describing the locations surrounding an individual point (the point of interest is at the centre of the matrix). Three variation of the LGM representation were considered: (i) level one LGMs where the eight closest surrounding neighbours are considered as shown in Figure 5a (this variation is described in previous work (El-Salhi et al., 2012)), (ii) level two LGMs where the eight surrounding neighbours "one step away" are considered as shown in Figure 5b and (iii) composite LGMs produced by combing level one and two LGMs as shown in Figure 5c. Two different options for generating the values to be stored in the LGM were also considered. The first option was to use the difference in height ($\delta z$) between the centre point $p_i$ and each of its $n$ neighbouring points $p_j$ ($1 \leq j \leq n$). The second was to use the angle, above or below the horizontal, between $p_i$ and each point $p_j$. Experimentation, described in (El-Salhi et al., 2012), indicated that composite LGMs coupled with $\delta z$ values proved to be the most effective representation. Whatever the case at the end of the process we have a LGM for each grid point. In the case of the training set this is augmented with an error value (calculated as described above). With respect to the LGM representation we



(a) Level one neighbourhood  (b) level two neighbourhood  (c) Composite neighbourhood
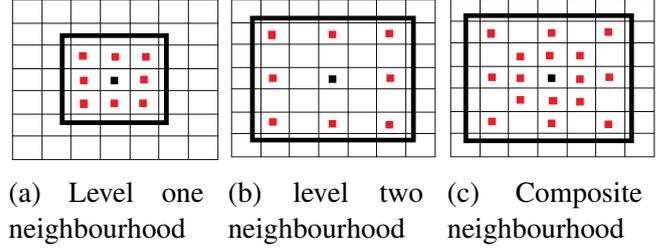
Figure 5: LGM configurations

opted for classifiers that operate using binary valued data, we therefore needed to discretise the data. To this end ranges of possible LGM values was replaced by one of a set of qualitative labels $L$ used to describes the nature of the slope in each of the eight directions. An example set of qualitative labels might be $\{n, l, p\}$ where $n$ indicates "negative", $l$ indicates "level" and $p$ indicates "positive". In the case of the training data required to generate a classifier, ranges of error values were used in a similar manner. Using this labelling, and by ordering the matrix elements (grid points) in a clockwise direction from the top left, a training set record might be described as follows:

$$\langle p, p, p, l, n, n, n, l, e \rangle$$

where $e$ is the associated springback. In this manner a dataset comprising a collection of LGM "feature vectors" could be constructed to which any one of a number of classifiers could be applied.

## 5. Local Distance Measure (LDM) Representation

The second 3D surface representation mechanism presented in this paper is the Local Distance Measure (LDM) mechanisms. This is founded on the observation that springback is greater further from edges (Behera et al., 2013). The idea is therefore to describe each grid square in terms of the distance from its centre to the nearest "critical feature point", where a critical feature point is a grid square that represents an edge of some kind. Thus the LDM process commences with the identification of the critical feature points in the input. This was achieved by identifying the eight angular differences $\alpha_1, \alpha_2, ..., \alpha_8$ between the normal to each centre point and its surrounding neighbourhood normals $\{E, NE, N, NW, W, SW, S,$

$SE$}. If one or more of the angular difference $\alpha_i$ was found to be greater than some tolerance measure, $\xi$, then the centre grid point was considered to be a critical feature point. Once the critical feature points had been detected the closest critical point to each grid centre point was determined by adopting a "region growing" process.

| The grid size $d$ | The tolerance value $\xi$ |
|:---:|:---:|
| 2.5 | 9 |
| 5 | 9 |
| 10 | 15 |
| 15 | 18 |
| 20 | 20 |

Table 1: The most appropriate tolerance value $\xi$ for different grid sizes ($d$) in the context of critical feature point detection

Equation 2 was used to calculate the minimum distance between the centre grid point $p_1 = (x_1, y_1, z_1)$ and the closest critical point $p_2 = (x_2, y_2, z_2)$.

$$d(p_1, p_2) = \sqrt{(x_1 - x_2)^2 + (y_1 - y_2)^2 + (z_1 - z_2)^2} \tag{2}$$

The result is a set of records each describing a grid square location in terms of its critical distance (and, in the case of a training set, its associated springback vale $E$). Clearly, there are two main factors that affect the process of edge detection: (i) the tolerance value $\xi$ and (ii) the grid size $d$. As the value for $\xi$ increases the number of identified critical feature points will decrease. As the grid size $d$ increases the number of identified critical feature points is also likely to increase because the angular differences between normals is more likely to be large. Consequently, in the context of the LDM representation, the $\xi$ and $d$ values are related and should be chosen carefully. An additional set of experiments, not reported in this paper (but see El-Salhi et al. (2012)), was conducted to identify the most appropriate value of $\xi$ to be associated with each $d$ value. Table 1 presents the main findings of these experiments, these are then the $\xi$ values used with respect to the evaluation reported later in this paper. The outcomes

when using $d = 2.5$mm and a number of different $\xi$ values ({15, 12, 9, 5}) to detect critical feature points (edges) in a flat-topped pyramid shape are presented in Figures 6, 7, 8 and 9. From the figures it can be seen $\xi = 9$ produces the best performance, when $\xi > 9$ critical feature points remain undiscovered, when $\xi < 9$ the system become too sensitive and too many points are identified.

Whatever the case, as in the case of the LGM representation, at the end of the process a dataset comprising a collection of LDM "feature vectors" is obtained to which a number of different possible classifiers can be applied.

## 6. Point Series Representation (PS)

This section presents the PS technique whereby a 3D surface is defined in terms of the local geometries surrounding individual grid square neighbourhoods based on the idea of linearising the key elements of the volume to form a sequence (series) of points. Thus the local,geometry for each grid square will be defined in terms of a point series. The desired linearisation can be conducted using a horizontal, vertical, "zig-zag" or a spiral linearisation so as to pass through each "key" grid point within a $n \times n$ neighbourhood centred on the grid square of interest as shown in Figure 10. With respect to the work described in this paper a spiral linearisation was used as also shown in Figure 10, the numbering indicate the ordering of the linearisation. This linearisation is translated to a curve representation where the x-axis gives the grid square number and the y-axis the $\delta z$ value associated with this grid square. In this manner we can generate a point series for each centre point $p_j$ located in grid $G_{in}$. In the context of training data each point series was also have associated with it an error label indicating the associated springback value $e_i$.

Using this point series representation we can create a "bank" of point series, each associated with an error value, which can be used to assign error values to the point series associated with new, previously unseen, surfaces. The $k$-Nearest Neighbour algorithm ($k$-NN) was used for this purpose. $k = 1$ was used to select the "nearest" curve in our point series bank to a new curve. Dynamic Time Warping
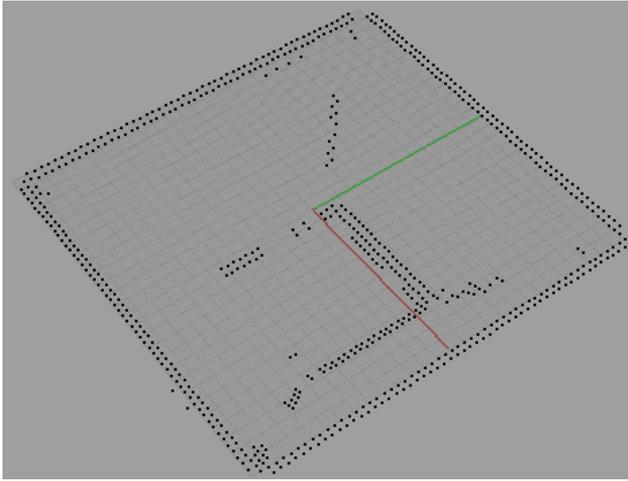
Figure 6: Critical feature point detection in a flat topped pyramid shape ($d = 2.5$ mm and $\xi = 15$).
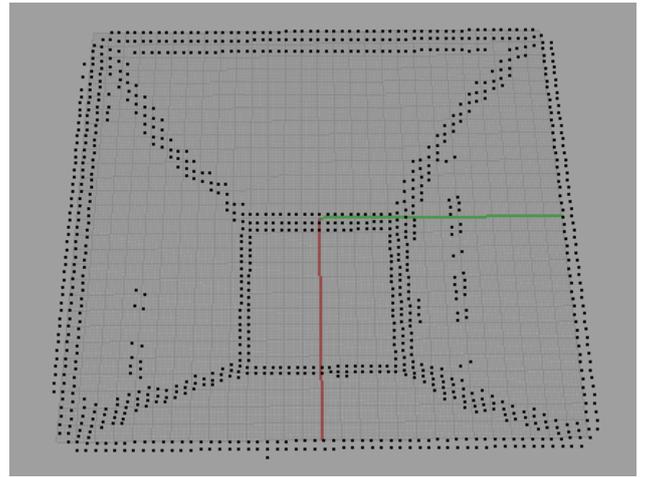


Figure 7: Critical feature point detection in a flat topped pyramid shape ($d = 2.5$ mm and $\xi = 12$).
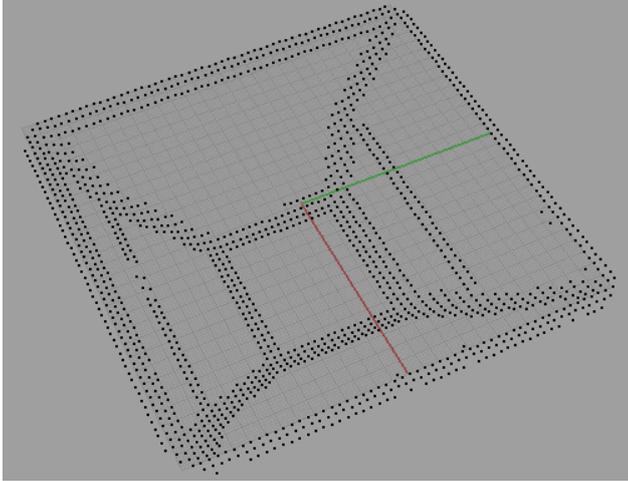


Figure 8: Critical feature point detection in a flat topped pyramid shape ($d = 2.5$ mm and $\xi = 9$).
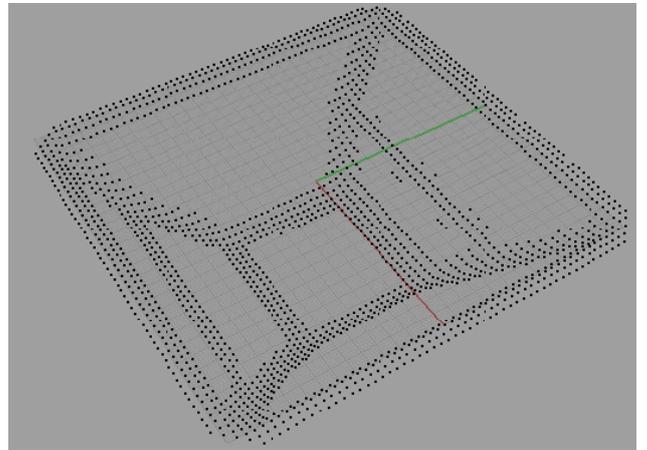


Figure 9: Critical feature point detection in a flat topped pyramid shape ($d = 2.5$ mm and $\xi = 5$).

(DTW) was adopted (Figure 11). DTW operates as follows. Given two point series $A = \{a_1, a_2, \cdots, a_n\}$ and $B = \{b_1, b_2, \cdots, b_m\}$, a matrix $T$ that has a dimension of $|A| \times |B| = n \times m$ is generated, where the value of the $(i^{th}, j^{th})$ element is obtained according to the Euclidean distance measure (absolute value of distance between two points) $d(i^{th}, j^{th}) = |a_i - b_j|$. After the matrix elements are computed, the similarity between two time series (curves) is defined in terms of the length of the "minimum path" across the matrix $T$ from the bottom-left to the top-right corner as shown in Figure 11. Thus the minimum DTW path between $A$ and $B$ is defined as follows:

$$min \; DTW \; path(A,B) = min\left(\sqrt{\sum_{k=1}^{K} w_k}\right) \quad (3)$$

where $w_k = d(i^{th}, j^{th})$ and $max(n,m) \leq K < m+n-1$ (Keogh & Pazzani, 2001; Xi et al., 2006). Note that given two identical curves the shortest path will be along the diagonal and the accumulated distance will be zero.

## 7. Evaluation

The comparison of the proposed methods was conducted using two flat-topped pyramid surfaces (shapes) referred to as the *Gonzalo* and *Modified* pyramids (see Figures 12 and 13). From the figures it can be observed that the two surfaces are similar although not identical (one side of the Gonzalo pyramid features a "bulge"). Some statistical characteristics for the $G_{in}$ grid, with respect to the two shapes, are presented in Table 2. Note that the Modified pyramid features many more points (although both pyramids are similar in size). Each surface was manufactured four times, twice in Steel and twice in Titanium. Hence, we have eight $G_{out}$ grids: (i) Gonzalo steel 1 (GS1), (ii) Gonzalo Steel 2 (GS2), (iii) Gonzalo titanium 1 (GT1), (iv) Gonzalo titanium 2 (GT2), (v) Modified steel 1 (MS1), (vi) Modified Steel 2 (MS2), (vii) Modified titanium 1 (MT1) and (viii) Modified titanium 2 (MT2). Some statistics concerning the $G_{out}$ grids are presented in Table 3.

The evaluation was conducted using a range of grid sizes $d = \{2.5, 5, 10, 15, 20\}$ (*mm*). Consequently
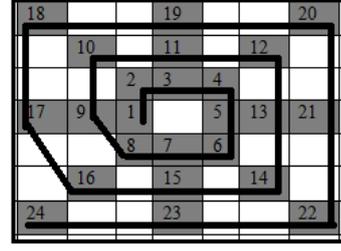


Figure 10: Spiral linearisation process for $7 \times 7$ patterns.
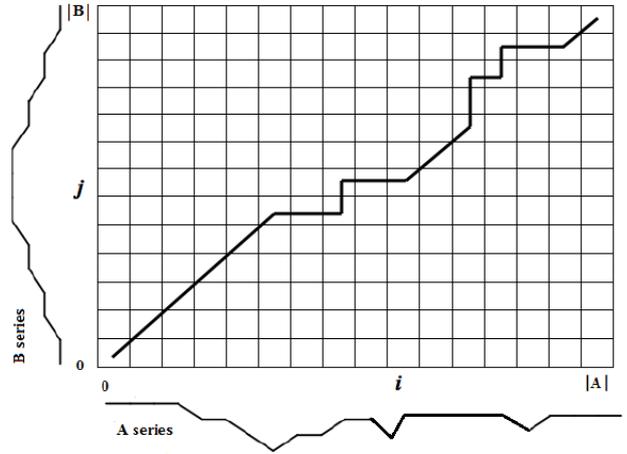


Figure 11: The minimum path between $A$ and $B$ series shown in by the bold diagonal line.

Table 2: Statistical characteristics for the $G_{in}$ point clouds for the Gonzalo and Modified pyramids: $W$ = width *mm*, $L$ = length *mm*, $H$ = height *mm*, $A$ = area of grid $(W \times L)$ $mm^2$, $N$ = number of points and $D$ = density of points per $mm^2$ $(N/A)$.

| $C_{in}$ | $W$ | $L$ | $H$ | $A$ | $N$ | $D$ |
|---|---|---|---|---|---|---|
| Gonzalo | 195 | 195 | 43 | 38025 | 250847 | 7.00 |
| Modified | 190 | 190 | 42 | 36100 | 565817 | 16.00 |

9
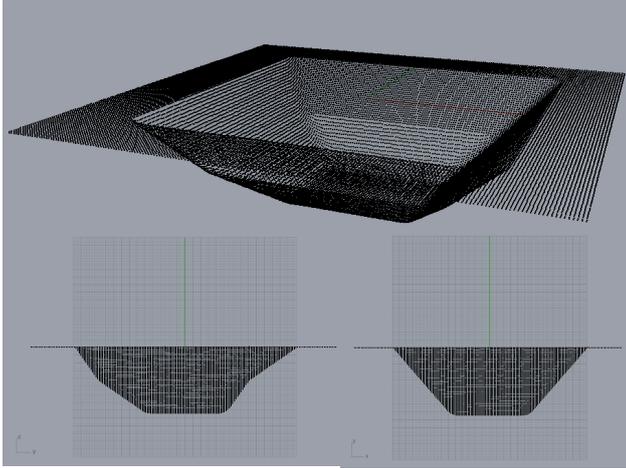
Figure 12: The $G_{in}$ cloud for Gonzalo steel pyramid.
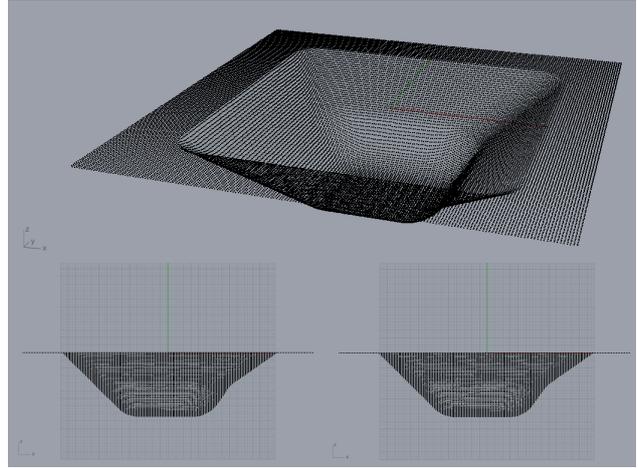


Figure 13: The $G_{in}$ cloud for Modified steel pyramid.

Table 3: Statistical characteristics for the $C_{out}$ point clouds for the Gonzalo and Modified pyramids.

| $C_{out}$ | W | L | H | A | N | D |
|-----------|-----|-----|-----|-------|--------|-------|
| GS1 | 194 | 194 | 45 | 37636 | 421214 | 11.00 |
| GS2 | 194 | 194 | 44 | 37636 | 233480 | 6.00 |
| GT1 | 199 | 189 | 46 | 37611 | 430900 | 11.00 |
| GT2 | 195 | 194 | 46 | 37830 | 185526 | 5.00 |
| MS1 | 196 | 195 | 45 | 38220 | 257436 | 7.00 |
| MS2 | 196 | 195 | 44 | 38220 | 269031 | 7.00 |
| MT1 | 195 | 195 | 47 | 38025 | 394895 | 10.00 |
| MT2 | 195 | 194 | 46 | 37830 | 401186 | 11.00 |

the number of generated records (recall that one record represents one grid square) varied for each data set according to the value of $d$, as shown in Table 4. For the PS representation a "tolerance" of 0.08 mm, as suggested by BS EN ISO 1101:2005 (BS ISO 1101), was used[2]. Recall also that a Decision Tree (DT) classifier was adopted with respect to the LGM and LDM techniques (although any other compatible classifier would have been equally appropriate), while $k$-NN coupled with DTW was used with respect to the PS technique. The results obtained are presented, in terms of both accuracy and Area Under ROC Curve (AUC), in Section 7.1 below.

_____

[2]BS EN ISO 1101 is a geometrical Product Specification (GPS) standards. The maximum variation between the technical design and actual (true) geometry is specified according to *tolerance* values included in the specification.

The first two objectives of the experiments were as follows: (i) to identify the most appropriate grid size with respect to each proposed technique and (ii) to identify the most appropriate 3D representation technique for springback prediction. Both these two objectives are discussed, with respect to the results reported in Sections 7.1, 7.2 and 7.3. Additional experiments were conducted to determine w-hether it was possible to generate a generic classifier, one trained on some suitable shape that could be used to predict the springback associated with other shapes. This is discussed further in Section 7.4. Further analysis is presented in Section 7.5, with respect to the second objective, to determine whether the results obtained are indeed statistically significant.

Table 4: Number of records generated for the Gonzalo and Modified pyramids using different values of $d$ (*mm*).

| $d$ | GS1 | GS2 | GT1 | GT2 | MS1 | MS2 | MT1 | MT2 |
|-----|------|------|------|------|------|------|------|------|
| 2.5 | 6086 | 6086 | 5928 | 6086 | 5853 | 5853 | 5853 | 5853 |
| 5 | 1523 | 1523 | 1483 | 1523 | 1483 | 1483 | 1483 | 1483 |
| 10 | 402 | 402 | 381 | 402 | 381 | 381 | 381 | 381 |
| 15 | 171 | 171 | 171 | 171 | 171 | 171 | 171 | 171 |
| 20 | 102 | 102 | 102 | 102 | 102 | 102 | 102 | 102 |

*7.1. Results*

This section presents the results obtained using the three proposed techniques and their variations and

a range of grid sizes $d = \{2.5, 5, 10, 15, 20\}$ (*mm*). In the case of the LGM technique a label size of $|L| = 3$ was used as earlier experiments (not reported here) demonstrated that this produced good results. The accuracy and AUC results obtained using the three LGM variations (Level 1 LGM, Level 2 LGM and the Composite LGM) are presented in Tables 5 and 6 respectively, best results are indicated in bold font. With respect to the LDM technique and the considered combinations of the LDM technique with the LGM technique (LDM+Level 1 LGM, LDM+Level 2 LGM and LDM+Composite LGM) Table 7 presents the accuracy results while Table 8 the AUC results (again best results are indicated using a bold font). For the Point Series (PS) technique a range of $n$ values, describing different $n \times n$ neighbourhood configurations ($n = \{3, 5, 7\}$), were considered. Recall that the PS technique was used in conjunction with $k$-NN classification and that a tolerance value of 0.08 mm was used when determining the DTW similarity between surfaces. Table 9 presents the accuracy results obtained while Table 10 presents the AUC results. The relevance of these results, with respect to the first two evaluation objectives, are presented in the following two sections; Section 7.2 and Section 7.3 respectively.

## 7.2. Best grid size

This section considers the results presented in the foregoing sections with respect to the identification of the most appropriate grid size, in the context of prediction effectiveness (AUC), with respect to each proposed techniques. The AUC measure was used for this purpose because it takes into account class priors, whilst the accuracy metric does not, AUC is therefore argued to be a better indicator of classification effectiveness. The three LGM variations (Level 1 LGM, Level 2 LGM and the Composite LGM) are considered in Section 7.2.1, the LDM technique and combinations of the LDM and LGM techniques (LDM + Level 1 LGM, LDM + Level 2 LGM, LDM + Composite LGM ) are discussed in Section 7.2.2 and the Point Series (PS) technique in Section 7.2.3.

## 7.2.1. The Best Grid size for LGM Technique

Considering the LGM technique and its variations first, from Table 5 it can be observed that high

Table 5: Accuracy results obtained using variations of the LGM representation using a range of values for grid size ($d = \{2.5, 5, 10, 15, 20\}$ mm and $|L| = 3$.

| Data Set | 3D Proposed Technique | Grid size ($d$) mm | | | | |
|---|---|---|---|---|---|---|
| | | 2.5 | 5 | 10 | 15 | 20 |
| GS1 | Level 1 LGM | 0.60 | 0.61 | 0.62 | 0.62 | **0.70** |
| | Level 2 LGM | 0.60 | 0.61 | **0.70** | 0.65 | 0.54 |
| | Composite LGM | 0.60 | 0.61 | 0.69 | 0.69 | 0.65 |
| GS2 | Level 1 LGM | 0.83 | 0.84 | 0.85 | 0.88 | **0.94** |
| | Level 2 LGM | 0.83 | 0.84 | 0.88 | 0.87 | 0.84 |
| | Composite LGM | 0.83 | 0.84 | 0.89 | 0.89 | 0.93 |
| GT1 | Level 1 LGM | 0.70 | 0.70 | 0.63 | **0.83** | 0.78 |
| | Level 2 LGM | 0.70 | 0.70 | 0.65 | 0.75 | 0.78 |
| | Composite LGM | 0.70 | 0.70 | 0.66 | 0.77 | 0.81 |
| GT2 | Level 1 LGM | 0.74 | 0.76 | 0.73 | 0.76 | 0.75 |
| | Level 2 LGM | 0.74 | 0.76 | 0.76 | 0.79 | 0.73 |
| | Composite LGM | 0.74 | 0.76 | 0.76 | **0.85** | 0.78 |
| MS1 | Level 1 LGM | 0.65 | 0.68 | 0.68 | 0.83 | **0.89** |
| | Level 2 LGM | 0.65 | 0.68 | 0.73 | 0.78 | 0.75 |
| | Composite LGM | 0.65 | 0.68 | 0.73 | 0.86 | 0.86 |
| MS2 | Level 1 LGM | 0.62 | 0.67 | 0.74 | 0.83 | 0.93 |
| | Level 2 LGM | 0.62 | 0.67 | 0.78 | 0.79 | 0.78 |
| | Composite LGM | 0.62 | 0.67 | 0.78 | 0.88 | **0.95** |
| MT1 | Level 1 LGM | 0.49 | 0.55 | 0.62 | 0.54 | 0.64 |
| | Level 2 LGM | 0.49 | 0.55 | **0.72** | 0.61 | 0.51 |
| | Composite LGM | 0.49 | 0.55 | **0.72** | 0.68 | 0.62 |
| MT2 | Level 1 LGM | 0.54 | 0.54 | 0.59 | 0.64 | **0.73** |
| | Level 2 LGM | 0.54 | 0.54 | 0.67 | 0.71 | 0.69 |
| | Composite LGM | 0.54 | 0.54 | 0.66 | 0.67 | 0.71 |
| Average | *Level 1 LGM* | 0.65 | 0.67 | 0.68 | 0.74 | **0.80** |
| | *Level 2 LGM* | 0.65 | 0.67 | 0.74 | 0.74 | 0.70 |
| | *Composite LGM* | 0.65 | 0.67 | 0.74 | 0.79 | 0.79 |

11

Table 6: AUC results obtained using variations of the LGM representation using a range of values for ford size ($d = \{2.5, 5, 10, 15, 20\}$ mm) and $|L| = 3$.

| Data Set | 3D Proposed Technique | Grid size ($d$) mm | | | | |
|---|---|---|---|---|---|---|
| | | 2.5 | 5 | 10 | 15 | 20 |
| GS1 | Level 1 LGM | 0.66 | 0.67 | 0.62 | 0.73 | **0.78** |
| | Level 2 LGM | 0.66 | 0.67 | 0.73 | 0.69 | 0.71 |
| | Composite LGM | 0.66 | 0.67 | 0.73 | 0.75 | 0.76 |
| GS2 | Level 1 LGM | 0.82 | 0.83 | 0.83 | 0.88 | 0.94 |
| | Level 2 LGM | 0.82 | 0.83 | **0.96** | 0.86 | 0.84 |
| | Composite LGM | 0.82 | 0.83 | **0.96** | 0.93 | 0.92 |
| GT1 | Level 1 LGM | 0.74 | 0.74 | 0.69 | 0.81 | 0.81 |
| | Level 2 LGM | 0.74 | 0.74 | 0.79 | 0.79 | **0.83** |
| | Composite LGM | 0.74 | 0.74 | 0.80 | **0.83** | **0.83** |
| GT2 | Level 1 LGM | 0.76 | 0.77 | 0.73 | 0.82 | 0.84 |
| | Level 2 LGM | 0.76 | 0.77 | 0.82 | 0.80 | 0.80 |
| | Composite LGM | 0.76 | 0.77 | 0.82 | **0.89** | 0.87 |
| MS1 | Level 1 LGM | 0.69 | 0.70 | 0.66 | 0.84 | 0.86 |
| | Level 2 LGM | 0.69 | 0.70 | 0.78 | 0.84 | 0.82 |
| | Composite LGM | 0.69 | 0.70 | 0.78 | **0.88** | 0.85 |
| MS2 | Level 1 LGM | 0.68 | 0.70 | 0.76 | 0.86 | **0.95** |
| | Level 2 LGM | 0.68 | 0.70 | 0.91 | 0.87 | 0.84 |
| | Composite LGM | 0.68 | 0.70 | 0.91 | 0.88 | 0.94 |
| MT1 | Level 1 LGM | 0.50 | 0.64 | 0.67 | 0.71 | 0.68 |
| | Level 2 LGM | 0.50 | 0.64 | 0.75 | 0.80 | 0.64 |
| | Composite LGM | 0.50 | 0.64 | 0.75 | **0.84** | 0.72 |
| MT2 | Level 1 LGM | 0.64 | 0.63 | 0.64 | 0.69 | 0.76 |
| | Level 2 LGM | 0.64 | 0.63 | 0.74 | **0.84** | 0.76 |
| | Composite LGM | 0.64 | 0.63 | 0.73 | **0.84** | 0.81 |
| Average | *Level 1 LGM* | 0.69 | 0.71 | 0.70 | 0.79 | 0.83 |
| | *Level 2 LGM* | 0.69 | 0.71 | 0.81 | 0.81 | 0.78 |
| | *Composite LGM* | 0.69 | 0.71 | 0.81 | **0.86** | 0.84 |

Table 7: Accuracy results obtained using variations of the LDM representation using a range of values for grid size ($d = \{2.5, 5, 10, 15, 20\}$ mm).

| Data Set | 3D Proposed Technique | Grid size ($d$) mm | | | | |
|---|---|---|---|---|---|---|
| | | 2.5 | 5 | 10 | 15 | 20 |
| GS1 | LDM | 0.50 | 0.53 | 0.54 | 0.54 | 0.45 |
| | LDM+Level 1 LGM | 0.62 | 0.63 | 0.62 | 0.65 | 0.68 |
| | LDM+Level 2 LGM | 0.62 | 0.63 | **0.71** | 0.66 | 0.54 |
| | LDM+Composite LGM | 0.62 | 0.63 | 0.70 | 0.66 | 0.65 |
| GS2 | LDM | 0.60 | 0.59 | 0.63 | 0.63 | 0.64 |
| | LDM+Level 1 LGM | 0.83 | 0.84 | 0.87 | 0.86 | **0.94** |
| | LDM+Level 2 LGM | 0.83 | 0.84 | 0.90 | 0.85 | 0.84 |
| | LDM+Composite LGM | 0.83 | 0.84 | 0.92 | 0.89 | 0.93 |
| GT1 | LDM | 0.51 | 0.53 | 0.64 | 0.49 | 0.55 |
| | LDM+Level 1 LGM | 0.70 | 0.70 | 0.64 | **0.82** | 0.78 |
| | LDM+Level 2 LGM | 0.70 | 0.70 | 0.68 | 0.81 | 0.77 |
| | LDM+Composite LGM | 0.70 | 0.70 | 0.68 | **0.82** | 0.81 |
| GT2 | LDM | 0.51 | 0.52 | 0.52 | 0.49 | 0.54 |
| | LDM+Level 1 LGM | 0.74 | 0.76 | 0.72 | 0.75 | 0.74 |
| | LDM+Level 2 LGM | 0.74 | 0.76 | 0.77 | 0.79 | 0.78 |
| | LDM+Composite LGM | 0.74 | 0.76 | 0.77 | **0.85** | 0.78 |
| MS1 | LDM | 0.55 | 0.54 | 0.55 | 0.62 | 0.64 |
| | LDM+Level 1 LGM | 0.68 | 0.68 | 0.70 | 0.86 | **0.89** |
| | LDM+Level 2 LGM | 0.68 | 0.68 | 0.72 | 0.82 | 0.75 |
| | LDM+Composite LGM | 0.68 | 0.68 | 0.73 | 0.88 | 0.86 |
| MS2 | LDM | 0.53 | 0.53 | 0.64 | 0.65 | 0.63 |
| | LDM+Level 1 LGM | 0.64 | 0.68 | 0.74 | 0.87 | 0.93 |
| | LDM+Level 2 LGM | 0.64 | 0.68 | 0.79 | 0.86 | 0.54 |
| | LDM+Composite LGM | 0.64 | 0.68 | 0.79 | 0.87 | **0.94** |
| MT1 | LDM | 0.59 | 0.55 | 0.52 | 0.44 | 0.54 |
| | LDM+Level 1 LGM | 0.59 | 0.57 | 0.62 | 0.58 | 0.64 |
| | LDM+Level 2 LGM | 0.59 | 0.57 | **0.72** | 0.61 | 0.56 |
| | LDM+Composite LGM | 0.59 | 0.57 | **0.72** | 0.68 | 0.59 |
| MT2 | LDM | 0.52 | 0.46 | 0.45 | 0.55 | 0.58 |
| | LDM+Level 1 LGM | 0.59 | 0.57 | 0.58 | 0.66 | **0.73** |
| | LDM+Level 2 LGM | 0.59 | 0.57 | 0.67 | 0.71 | 0.68 |
| | LDM+Composite LGM | 0.59 | 0.57 | 0.67 | 0.67 | 0.71 |
| Average | *LDM* | 0.54 | 0.53 | 0.56 | 0.55 | **0.57** |
| | *LDM+ Level 1 LGM* | 0.67 | 0.68 | 0.69 | 0.76 | **0.79** |
| | *LDM+ Level 1 LGM* | 0.67 | 0.68 | 0.75 | 0.76 | 0.71 |
| | *LDM+ Composite LGM* | 0.67 | 0.68 | 0.75 | **0.79** | 0.78 |

Table 8: AUC results obtained using variations of the LDM representation using a range of values for grid size ($d = \{2.5, 5, 10, 15, 20\}$ mm).

| Data Set | 3D Proposed Technique | Grid size ($d$) mm | | | | |
|---|---|---|---|---|---|---|
| | | 2.5 | 5 | 10 | 15 | 20 |
| GS1 | LDM | 0.50 | 0.51 | 0.50 | 0.49 | 0.46 |
| | LDM+Level 1 LGM | 0.69 | 0.68 | 0.65 | 0.73 | **0.76** |
| | LDM+Level 2 LGM | 0.69 | 0.68 | 0.75 | 0.72 | 0.71 |
| | LDM+Composite LGM | 0.69 | 0.68 | 0.74 | 0.75 | 0.75 |
| GS2 | LDM | 0.50 | 0.50 | 0.47 | 0.47 | 0.45 |
| | LDM+Level 1 LGM | 0.82 | 0.83 | 0.84 | 0.90 | 0.94 |
| | LDM+Level 2 LGM | 0.82 | 0.83 | 0.95 | 0.86 | 0.84 |
| | LDM+Composite LGM | 0.82 | 0.83 | **0.96** | 0.93 | 0.92 |
| GT1 | LDM | 0.53 | 0.54 | 0.45 | 0.49 | 0.61 |
| | LDM+Level 1 LGM | 0.74 | 0.74 | 0.71 | 0.82 | 0.80 |
| | LDM+Level 2 LGM | 0.74 | 0.74 | 0.79 | 0.81 | 0.84 |
| | LDM+Composite LGM | 0.74 | 0.74 | 0.80 | **0.85** | 0.83 |
| GT2 | LDM | 0.50 | 0.50 | 0.45 | 0.53 | 0.45 |
| | LDM+Level 1 LGM | 0.76 | 0.77 | 0.72 | 0.81 | 0.84 |
| | LDM+Level 2 LGM | 0.76 | 0.77 | 0.81 | 0.80 | 0.80 |
| | LDM+Composite LGM | 0.76 | 0.77 | 0.81 | **0.88** | 0.87 |
| MS1 | LDM | 0.57 | 0.50 | 0.54 | 0.47 | 0.45 |
| | LDM+Level 1 LGM | 0.71 | 0.70 | 0.74 | 0.85 | 0.86 |
| | LDM+Level 2 LGM | 0.71 | 0.70 | 0.80 | 0.87 | 0.82 |
| | LDM+Composite LGM | 0.71 | 0.70 | 0.80 | **0.88** | 0.85 |
| MS2 | LDM | 0.58 | 0.50 | 0.49 | 0.48 | 0.45 |
| | LDM+Level 1 LGM | 0.71 | 0.71 | 0.75 | 0.87 | 0.96 |
| | LDM+Level 2 LGM | 0.71 | 0.71 | 0.92 | 0.90 | 0.84 |
| | LDM+Composite LGM | 0.71 | 0.71 | 0.92 | 0.87 | **0.97** |
| MT1 | LDM | 0.50 | 0.52 | 0.50 | 0.49 | 0.55 |
| | LDM+Level 1 LGM | 0.68 | 0.67 | 0.67 | 0.75 | 0.68 |
| | LDM+Level 2 LGM | 0.68 | 0.67 | 0.75 | 0.80 | 0.68 |
| | LDM+Composite LGM | 0.68 | 0.67 | 0.75 | **0.84** | 0.71 |
| MT2 | LDM | 0.59 | 0.50 | 0.49 | 0.58 | 0.57 |
| | LDM+Level 1 LGM | 0.68 | 0.67 | 0.64 | 0.73 | 0.76 |
| | LDM+Level 2 LGM | 0.68 | 0.67 | 0.75 | **0.86** | 0.77 |
| | LDM+Composite LGM | 0.68 | 0.67 | 0.75 | 0.85 | 0.80 |
| Average | *LDM* | 0.53 | 0.51 | 0.49 | 0.50 | 0.50 |
| | *LDM+ Level 1 LGM* | 0.72 | 0.72 | 0.72 | 0.81 | 0.83 |
| | *LDM+ Level 2 LGM* | 0.72 | 0.72 | 0.82 | 0.83 | 0.79 |
| | *LDM+ Composite LGM* | 0.72 | 0.72 | 0.82 | **0.86** | 0.84 |

Table 9: The Accuracy results obtained using variations of the the PS representation and a range of values for grid size ($d = \{2.5, 5, 10, 15, 20\}$ mm) and neighbourhood size ($n = \{3, 5, 7\}$).

| Data set | $n \times n$ PS | Grid size ($d$) mm | | | | |
|---|---|---|---|---|---|---|
| | | 2.5 | 5 | 10 | 15 | 20 |
| GS1 | $3 \times 3$ PS | 0.97 | **0.98** | **0.98** | 0.97 | 0.90 |
| | $5 \times 5$ PS | 0.97 | 0.97 | 0.98 | **1.00** | 0.84 |
| | $7 \times 7$ PS | 0.98 | **0.99** | 0.94 | 0.87 | 0.78 |
| GS2 | $3 \times 3$ PS | **0.99** | 0.98 | 0.97 | 0.96 | 0.96 |
| | $5 \times 5$ PS | **0.99** | 0.97 | 0.96 | 0.94 | 0.92 |
| | $7 \times 7$ PS | **0.99** | 0.98 | 0.94 | 0.89 | 0.67 |
| GT1 | $3 \times 3$ PS | 0.99 | **1.00** | 0.99 | 0.94 | 0.93 |
| | $5 \times 5$ PS | **0.99** | **0.99** | 0.94 | 0.94 | 0.91 |
| | $7 \times 7$ PS | 0.98 | **0.99** | 0.87 | 0.79 | 0.81 |
| GT2 | $3 \times 3$ PS | **0.99** | **0.99** | **0.99** | 0.98 | 0.96 |
| | $5 \times 5$ PS | 0.99 | **0.99** | 0.96 | 0.95 | **0.99** |
| | $7 \times 7$ PS | **0.99** | 0.98 | 0.88 | 0.83 | 0.48 |
| MS1 | $3 \times 3$ PS | 0.97 | 0.97 | **0.98** | 0.97 | 0.97 |
| | $5 \times 5$ PS | 0.96 | 0.96 | 0.96 | **0.98** | 0.91 |
| | $7 \times 7$ PS | 0.96 | 0.97 | **0.99** | 0.89 | 0.75 |
| MS2 | $3 \times 3$ PS | 0.96 | **0.98** | **0.98** | 0.97 | 0.92 |
| | $5 \times 5$ PS | 0.96 | 0.96 | **0.97** | **0.97** | 0.92 |
| | $7 \times 7$ PS | **0.97** | **0.97** | 0.96 | 0.92 | 0.67 |
| MT1 | $3 \times 3$ PS | **0.98** | **0.98** | **0.98** | 0.97 | 0.90 |
| | $5 \times 5$ PS | **0.98** | **0.98** | 0.96 | 0.97 | 0.84 |
| | $7 \times 7$ PS | **0.98** | **0.98** | 0.92 | 0.97 | 0.70 |
| MT2 | $3 \times 3$ PS | 0.97 | 0.96 | 0.93 | **0.98** | 0.82 |
| | $5 \times 5$ PS | 0.97 | 0.96 | 0.93 | 0.96 | **0.99** |
| | $7 \times 7$ PS | **0.97** | 0.96 | **0.97** | 0.92 | 0.56 |
| Avergae | $3 \times 3$ PS | **0.98** | **0.98** | **0.98** | 0.97 | 0.92 |
| | $5 \times 5$ PS | **0.98** | **0.98** | 0.96 | 0.96 | 0.92 |
| | $7 \times 7$ PS | **0.98** | **0.98** | 0.93 | 0.89 | 0.68 |

13

Table 10: The AUC results obtained using variations of the the PS representation and a range of values for grid size ($d = \{2.5, 5, 10, 15, 20\}$ mm) and neighbourhood size ($n = \{3, 5, 7\}$).

| Data set | $n \times n$ PS | Grid size ($d$) mm | | | | |
|---|---|---|---|---|---|---|
| | | 2.5 | 5 | 10 | 15 | 20 |
| GS1 | 3 × 3 PS | 0.96 | **0.97** | 0.96 | 0.95 | 0.82 |
| | 5 × 5 PS | 0.96 | 0.95 | 0.97 | **1.00** | 0.80 |
| | 7 × 7 PS | 0.97 | **0.98** | 0.92 | 0.70 | 0.33 |
| GS2 | 3 × 3 PS | **0.94** | 0.89 | 0.84 | 0.64 | 0.78 |
| | 5 × 5 PS | **0.94** | 0.89 | 0.75 | 0.64 | 0.73 |
| | 7 × 7 PS | **0.96** | 0.93 | 0.85 | 0.65 | 0.50 |
| GT1 | 3 × 3 PS | 0.97 | **1.00** | 0.98 | 0.76 | 0.72 |
| | 5 × 5 PS | 0.96 | **0.99** | 0.89 | 0.70 | 0.74 |
| | 7 × 7 PS | 0.93 | **0.99** | 0.77 | 0.57 | 0.89 |
| GT2 | 3 × 3 PS | 0.96 | **0.99** | 0.97 | 0.93 | 0.96 |
| | 5 × 5 PS | 0.96 | 0.98 | 0.85 | 0.90 | **0.99** |
| | 7 × 7 PS | 0.95 | **0.96** | 0.72 | 0.75 | 0.19 |
| MS1 | 3 × 3 PS | 0.92 | 0.92 | **0.97** | 0.94 | 0.87 |
| | 5 × 5 PS | 0.91 | 0.92 | 0.92 | **0.97** | 0.62 |
| | 7 × 7 PS | 0.92 | 0.95 | **0.99** | 0.81 | 0.67 |
| MS2 | 3 × 3 PS | 0.94 | **0.97** | 0.93 | 0.92 | 0.71 |
| | 5 × 5 PS | **0.94** | 0.94 | 0.91 | 0.93 | 0.64 |
| | 7 × 7 PS | 0.95 | **0.97** | 0.95 | 0.86 | 0.50 |
| MT1 | 3 × 3 PS | 0.96 | **0.97** | 0.94 | 0.96 | 0.81 |
| | 5 × 5 PS | **0.96** | 0.96 | 0.89 | 0.95 | 0.70 |
| | 7 × 7 PS | 0.95 | 0.97 | 0.72 | **1.00** | 0.47 |
| MT2 | 3 × 3 PS | **0.96** | 0.94 | 0.90 | 0.94 | 0.73 |
| | 5 × 5 PS | 0.96 | 0.94 | 0.92 | 0.93 | **0.98** |
| | 7 × 7 PS | 0.94 | 0.93 | **0.95** | 0.74 | 0.25 |
| Avergae | 3 × 3 PS | 0.95 | **0.96** | 0.94 | 0.88 | 0.95 |
| | 5 × 5 PS | 0.95 | 0.95 | 0.89 | 0.88 | 0.78 |
| | 7 × 7 PS | 0.95 | **0.96** | 0.86 | 0.76 | 0.48 |

grid sizes tended to produces better accuracy results (best accuracy of 0.95% when $d = 20$), although when $d$ is large the data sets comprise fewer records than when $d$ is small. Similarly, from Table 6 it can be seen that most of the best AUC results were obtained using higher values of $d$ (best AUC of 0.96 when $d = 10$). A better understanding of the effect of grid size can be obtained by considering the number of occasions that a best AUC result was produced with respect to each $d$ value and each LGM variation. This is presented in Table 11. Note that because we have eight $C_{out}$ clouds (test sets) each row adds up to 8. From this table, it can be seen that the Level 1 LGM technique was able to represent effectively 3D surfaces using a large grid sizes ($d = 20$), while the Level 2 LGM technique required smaller grid size ($d = 10$) to be effective. However, the composite LGM operated best at a compromise $d$ value of 15 mm (recall that the composite LGM technique uses both Level 1 and Level 2 LGMs, a combination of the two).

Table 11: Number of times each grid size ($d = \{2.5, 5, 10, 15, 20\}$ mm) produced the best performance, in terms of AUC, with respect to each of the three LGM techniques considered and each of the eight data sets.

| Proposed Techniques | Grid size ($d$) mm | | | | | Best $d$ value |
|---|---|---|---|---|---|---|
| | 2.5 | 5 | 10 | 15 | 20 | |
| Level 1 LGM | 0 | 0 | 0 | 1.5 | **6.5** | 20 |
| Level 2 LGM | 0 | 0 | **4** | 3 | 1 | 10 |
| Composite LGM | 0 | 0 | 1 | **5.5** | 1.5 | 15 |

*7.2.2. The Best Grid size for LDM Technique*

With respect to the LDM technique, and the combinations with the LGM techniques, from Table 7 and 8 it can be observed that the best results were obtained using grid sizes of between $d = 10$ and $d = 20$ (best accuracy was 94% when $d = 20$, and best AUC was 0.97 when $d = 20$). Table 12 records the number of occasions that each grid size produced the best performance (in terms of AUC) with respect to each of the four LDM techniques and each of the eight data sets considered. From the table it can be seen that when the LDM technique is used in isolation

best results are obtained using low values of $d$ (although the results are not conclusive). When combing the LDM technique with LGM the best $d$ values are comparable with those obtained when using LGMs on their own.

Table 12: Number of times each grid size ($d = \{2.5, 5, 10, 15, 20\}$ mm) produced the best performance (in terms of AUC) with respect to each of the four LDM techniques considered and each of the eight data sets.

| Proposed Techniques | Grid size ($d$) mm | | | | | Best $d$ value |
|---|---|---|---|---|---|---|
| | 2.5 | 5 | 10 | 15 | 20 | |
| LDM | **3.5** | 1.5 | 0 | 1 | 2 | 2.5 |
| LDM+Level 1 LGM | 0 | 0 | 0 | 2 | **6** | 20 |
| LDM+Level 2 LGM | 0 | 0 | **4** | 3 | 1 | 10 |
| LDM+Composite LGM | 0 | 0 | 1 | **5** | 2 | 15 |

*7.2.3. The Best Grid size for PS Technique*

In the case of the Point Series (PS) technique Tables 9 and 10 indicate, although not entirely conclusively, that a grid size of $d = 5$ is the most appropriate. The number of occasions that each grid size produced the best AUC value, with respect to each PS variation and each data set considered, is shown in Table 13. The table confirms that the most appropriate grid size is $d = 5$. There is little to choose between the PS variations when $d$ is small; it is not until we get to $d = 20$ that some significant difference between the PS variations can be noted. With reference to Table 10 and when $d = 20$ the $3 \times 3$ configuration produced the best results (AUC=0.99) while the $7 \times 7$ configuration produced the worst results (AUC=0.19). Of course there is a relationship between $n$ and $d$, as either is increased a greater area of the surface of interest is "covered", increasing one and decreasing the other has a neutralising effect. Finally, all three techniques considered operate using different values of $d$ because in each case $d$ is being used in a different manner. With respect to LGMs we wish to set $d$ to a value which optimizes the area covered in terms of the description of the local geometry. With respect to LDMs we wish to set $d$ so as to optimize the discovery of edges. With respect to PS we

wish to set $d$ so that the nature of the point series is optimized with respect to classification performance.

Table 13: The occurrences of the best AUC results obtained by $3 \times 3$, $5 \times 5$ and $7 \times 7$ PS for a range of grid size $d = \{2.5, 5, 10, 15, 20\}$.

| PS Technique | Grid size ($d$) mm | | | | | Best $d$ value |
|---|---|---|---|---|---|---|
| | 2.5 | 5 | 10 | 15 | 20 | |
| $3 \times 3$ PS | 2 | **5** | 1 | 0 | 0 | 5 |
| $5 \times 5$ PS | **2** | **2** | 0 | **2** | **2** | 5 |
| $7 \times 7$ PS | 1 | **4** | 2 | 1 | 0 | 5 |

Table 14: Some statistics concerning the AUC results obtained from the application of the LGM techniques.

| LGM Techniques | Max | Min | Median | Average | SD |
|---|---|---|---|---|---|
| Level 1 LGM | 0.95 | 0.50 | 0.74 | 0.74 | 0.09 |
| Level 2 LGM | 0.96 | 0.50 | 0.77 | 0.76 | 0.09 |
| Composite LGM | 0.96 | 0.50 | 0.78 | 0.78 | 0.10 |

Table 15: Some statistics concerning the AUC results obtained from the application of the LDM technique (and its variations).

| LDM Techniques | Max | Min | Median | Average | SD |
|---|---|---|---|---|---|
| LDM | 0.61 | 0.45 | 0.50 | 0.51 | 0.04 |
| LDM+Level 1 LGM | 0.96 | 0.64 | 0.74 | 0.76 | 0.08 |
| LDM+Level 2 LGM | 0.95 | 0.67 | 0.77 | 0.78 | 0.07 |
| LDM+Composite LGM | 0.97 | 0.67 | 0.79 | 0.79 | 0.09 |

*7.3. Best Surface Representation Technique*

Tables 14, 15 and 16 present, respectively, some statistics concerning the operation of the LGM, LDM and PS techniques and their variations in terms of AUC. These statistics have been derived from Tables 5 to 10. In the context of the LGM techniques, from Table 14 it can be observed that the Composite LGM representation produces the most effective result (average AUC value of 0.78); although, in terms of classification, there is little to choose between them. With

Table 16: Some statistics concerning the AUC results obtained from the application of the PS technique.

| PS Techniques | Max | Min | Median | Average | SD |
|---|---|---|---|---|---|
| $3 \times 3$ PS | 1.00 | 0.64 | 0.94 | 0.90 | 0.09 |
| $5 \times 5$ PS | 1.00 | 0.62 | 0.93 | 0.89 | 0.10 |
| $7 \times 7$ PS | 1.00 | 0.19 | 0.92 | 0.92 | 0.22 |

respect to the LDM technique, from Table 15, it can be noted that the LDM technique on its own did not produce an effective performance compared to its usage when combined with the LGM technique. The best performance was obtained when LDM was combined with the Composite LGM representation (best average AUC value of 0.79). In the case of the PS technique Table 16 demonstrates that this technique produced excellent results, regardless of the size of the neighbourhood the PS technique outperformed the best performing variations of both the LGM and LDM techniques. Overall the most consistent PS technique (that with the smaller standard deviation) was when it was coupled with a $3 \times 3$ neighbourhood. Table 17 summarises the best variation for each category of representation technique (LDM is included in isolation and in combination with the Composite LGM technique).

Table 17: Summary *best* variation, with respect to AUC, for each representation technique (LDM is included in isolation and in combination with the Composite LGM technique).

| | Max | Min | Mode | Median | Average | SD |
|---|---|---|---|---|---|---|
| Composite LGM | 0.93 | 0.75 | 0.88 | 0.84 | 0.86 | 0.06 |
| LDM | 0.59 | 0.50 | 0.50 | 0.57 | 1.03 | 1.04 |
| LDM+Composite LGM | 0.93 | 0.75 | 0.85 | 0.85 | 0.86 | 0.07 |
| $3 \times 3$ PS | **1.00** | **0.96** | **0.98** | **0.98** | **0.98** | **0.01** |

### 7.4. Generalisation

This section presents the results obtained from training a classifier on one shape and testing it on another. The main goal was to determine whether it was possible to generate a generally applicable classifier if it was provided with a suitable shape to train on.

The $3 \times 3$ neighbourhood PS representation was used for this purpose (with $d = 5$ mm) because earlier experiments had indicated that this technique was the most effective (recall that the PS technique was used in conjunction with $k$-NN classification and that a tolerance value of 0.08 mm was used in the context of DTW similarity). Table 18 presents the results obtained in terms of accuracy values, while Table 19 presents the results obtained in terms of AUC values (best results are in bold). From the tables it can be observed again that using the proposed representation a best accuracy and AUC value of 100% and 1.00 could be obtained (when the classifier is trained using GS2). However, the best overall accuracy average was 0.99 while the best overall AUC average was 0.98. These are excellent results. The results obtained in terms of both AUC and accuracy also indicated that, no matter the nature of the 3D surface to be manufactured or the material from which it is to be manufactured, an effective generic classifier can be produced using the proposed PS technique.

Table 18: Accuracy results for the generic classifier based on $3 \times 3$ PS.

| | | Train | | | | | | | |
|---|---|---|---|---|---|---|---|---|---|
| | | GS1 | GS2 | GT1 | GT2 | MS1 | MS2 | MT1 | MT2 |
| Test | GS1 | | 0.96 | **0.99** | 0.98 | 0.95 | 0.89 | **0.99** | **0.99** |
| | GS2 | 0.98 | | **1.00** | 0.99 | 0.97 | 0.91 | **1.00** | 0.99 |
| | GT1 | 0.95 | 0.95 | | **0.97** | 0.88 | 0.89 | **0.97** | **0.97** |
| | GT2 | 0.95 | 0.98 | 0.98 | | 0.93 | 0.88 | **0.99** | 0.98 |
| | MS1 | 0.98 | **0.99** | **0.99** | **0.99** | | 0.95 | 0.98 | 0.98 |
| | MS2 | 0.96 | 0.97 | **0.99** | **0.99** | 0.98 | | 0.98 | 0.98 |
| | MT1 | 0.96 | 0.97 | **0.99** | 0.98 | 0.90 | 0.88 | | 0.98 |
| | MT2 | 0.96 | 0.98 | **0.99** | 0.97 | 0.90 | 0.87 | **0.99** | |
| Average | | 0.96 | 0.97 | **0.99** | 0.98 | 0.93 | 0.90 | **0.99** | 0.98 |

### 7.5. Statistical Analysis

This section presents a statistical significance comparison of four of the techniques considered: (i) the best LGM variation, Composite LGM, (ii) LDM used in isolation; (iii) the best variation of LDM when combined with the best LGM technique, LDM + Composite LGM; and (iv) the best PS variation, PS coupled with a $3 \times 3$ neighbourhood. The objective is to demonstrate that there is a statistical significance with respect to the comparative performance of the proposed techniques. To this end, the Friedman statistical test was applied to evaluate the performance

Table 19: AUC results for the generic classifier based on $3 \times 3$ PS.

| | | Train | | | | | | | |
|---|---|---|---|---|---|---|---|---|---|
| | | GS1 | GS2 | GT1 | GT2 | MS1 | MS2 | MT1 | MT2 |
| Test | GS1 | | 0.97 | 0.94 | 0.93 | 0.96 | 0.91 | 0.96 | **0.98** |
| | GS2 | 0.99 | | 0.99 | 0.92 | **1.00** | 0.96 | **1.00** | 0.99 |
| | GT1 | 0.84 | 0.87 | | **0.95** | 0.64 | 0.66 | 0.94 | 0.94 |
| | GT2 | 0.81 | 0.91 | 0.98 | | 0.65 | 0.61 | **0.99** | 0.95 |
| | MS1 | 0.98 | **0.99** | **0.99** | 0.98 | | 0.95 | 0.98 | 0.97 |
| | MS2 | 0.95 | 0.96 | 0.99 | **1.00** | 0.98 | | 0.97 | 0.97 |
| | MT1 | 0.85 | 0.88 | **0.96** | 0.94 | 0.62 | 0.59 | | 0.95 |
| | MT2 | 0.90 | **1.00** | 0.98 | 0.93 | 0.65 | 0.63 | 0.99 | |
| Average | | 0.90 | 0.94 | **0.98** | 0.95 | 0.79 | 0.76 | **0.98** | 0.96 |

of the techniques to determine whether the results produced were truly significant or not with respect to the AUC measure. On completion of the Friedman test, the Nemenyi test was used to identify the Critical Distance (CD) between the techniques where the techniques are significantly different from each other. Broadly, CD is normally used to examine where the significant differences are actually occured between *individual* techniques. This kind of statistical analysis is increasingly being used in the field of data mining and more specifically in the context of classification (Han, 2005; Tan et al., 2005). A number of different approaches have been proposed to conduct such comparisons. With respect to classification techniques the following are of note: (i) the paired t-test, (ii) the Wilcoxon Signed-Rank Test, (iii) the ANOVA test and (iv) the Friedman test[3]. The Friedman test offers two advantages over the other techniques: (i) ease of computation and interpretation and (ii) its ability to demonstrate the classification performance in terms of a ranking rather than vague averages (García et al., 2009b)). The Friedman test was thus chosen to evaluate the performance of the different proposed techniques with respect to this paper. In addition to the practical advantages offered by the Friedman test, it was also chosen because:

- There is no guarantee that the data (AUC results obtained from the proposed techniques) follow the normal (Gaussian) distribution.

---

[3]For more detail on these tests (García et al., 2009a,b; Tsumoto, 2009).

- It is recommended (Demšar, 2006) for use with "matched" (related) data sets while the ANOVA test is recommended for use with "unrelated" data sets.

With respect to the work described in this paper, the Gonzalo and Modified data sets were considered to be related data sets given that both describe flat-topped pyramids. Therefore, the Friedman test was considered to be the most suitable statistical test. Therefore, The following *Null hypothesis* ($H_0$) and the *Alternative hypothesis* ($H_1$) were established.

**H 0.** *There is no significant difference between the proposed classifiers.*

**H 1.** *There is a significant difference between the proposed classifiers.*

The Friedman statistical test is commenced by *ranking* the classification techniques with respect to each data set separately. Then, the average rank for each classification techniques is obtained from across the data sets. The Friedman test statistic is then calculated as follows (Demšar, 2006; Friedman, 1940; Fisher & Yates, 1970):

$$\chi_F^2 = \frac{12n}{k(k+1)} \left[ \sum_{i=1}^{k} \mu_i^2 - \frac{k(k+1)^2}{4} \right] \quad (4)$$

where: (i) $n$ is the number of data sets, (ii) $k$ is the number of classification techniques and (iii) $\mu_i$ is the average rank for classification technique $i$ which in turn is calculated as follows:

$$\mu_i = \frac{1}{n} \sum_{j=1}^{n} R_j \quad (5)$$

where $R_j$ is the rank for classification technique $i$ with respect to data set $j$. To decide weather the Friedman test statistic ($\chi_F^2$) value is significant or not it is compared with the null distribution (pre-determined theoretical distribution) calculated according to the $\chi^2$ distribution at $\alpha = 0.05$ (the most commonly used value to describe the level of significance $\alpha$ (Friedman, 1940; GW, 1983)). If the calculated value of $\chi_F^2$ is greater than the null distribution, then the null

hypothesis can be rejected and the Nemenyi test (Nemenyi, 1963) applied. The Nemenyi test operates using the "distance" between the average rankings of the individual techniques. If this distance is greater than a Critical Difference (CD), calculated using Equation 6, then the performance is considered to be distinct. To qualify the strength of evidences against the null hypothesis, a *p-value* is calculated. The *p-value* is defined as the probability of obtaining a result that is at least as extreme as the one we actually obtained assuming that the null hypothesis is true. Therefore, if the *p-value* is not smaller than $\alpha$, the test is inconclusive and more evidences will be required to support the alternative hypothesis (H1).

$$CD = q_{\alpha,\infty,k} \sqrt{\frac{k(k+1)}{12n}} \qquad (6)$$

Where the critical value for $q_{\alpha,\infty,k}$ is based on the Studentized range statistic (Demšar, 2006). The performance of individual techniques is considered to be distinct if the difference between their average rankings differs by at least the CD.

The Friedman test was applied with respect to the proposed techniques in the context of the evaluation data sets. Two different cases were considered: (i) where the classification techniques was trained and tested on the same data set and (ii) where the classification techniques was trained on one data set and tested on another. Each is considered in further detail in the following two sections.

### 7.5.1. Testing and training on the same dataset

The Friedman statistical test was first applied to our four different technique with respect to the $n = 8$ Gonzalo and Modified data sets (GS1, GS2, GT1, GT2, MS1, MS2, MT1 and MT2). Table 20 presents the rankings (indicated in parentheses) and the average ranks $\mu$ for the $k = 4$ proposed techniques (according to the best AUC values). From the table, it can be seen that the best average rank, 1.25, was achieved by the PS technique. The Friedman statistic, calculated using Equation 4 with $k - 1 = 3$ degrees of freedom, is then:

$$\chi_F^2 = \frac{12 \times 8}{4 \times (5)} \left[ 28.91 - \frac{4 \times (5)^2}{4} \right]$$
$$= 4.80 \times 3.91$$
$$= 18.77$$

The $\chi^2$ threshold value with $\alpha = 0.05$ and 3 degree of freedom (null distribution) is 14.07. Given that: (i) the calculated Friedman test value of $\chi_F^2 = 18.77$ is greater than the critical value 14.07, and (ii) *p-value* = 0.009 which is less than the $\alpha$ value of 0.05 (Abramowitz & I.A. Stegun, 1964; Johnson et al., 1995); the Null Hypothesis ($H_0$), which states that there is no significant differences in the average ranks, can be rejected to confirm that the operation of the $k = 4$ proposed classifiers generated on the same data sets are significantly different from each other. According to the Nemenyi test the operation of the individual classifiers is also significantly different if the difference between their average ranks is more than or equal $CD = 1.17$, calculated as follows:

$$CD = 2.57 \times \sqrt{\frac{4(5)}{12 \times 8}}$$
$$= 2.57 \times 0.46$$
$$= 1.17$$

Figure 14 shows the ranked performance for the $k = 4$ proposed techniques along with Nemenyis critical difference (CD) measure to highlight the techniques which are significantly different to each other. In the figure, the head is the average rank while the tail indicates the CD value. From the figure, it can be seen that the PS technique was ranked first and that its operation is significantly different with respect to both the LDM and the composite LGM techniques because as they are *overlapped*. However, there is no significant difference between the operation of PS and LDM + composite LGM as the difference between their average ranks is $0.88 < 1.17$ (the CD value).

### 7.5.2. Testing and training on different datasets

In the case where the classifier is generated (trained) on one data set and tested using another Table 21

Table 20: The best AUC results for the proposed techniques (variations) with respect to each 3D representation technique using the same data set to train and test the classifier.

| | GS1 | GS2 | GT1 | GT2 | MS1 | MS2 | MT1 | MT2 | $\mu_i$ |
|---|---|---|---|---|---|---|---|---|---|
| Composite LGM | 0.73 (3) | **0.96 (1.5)** | 0.80 (2.5) | 0.82 (2) | 0.78 (3) | 0.91 (3) | 0.75 (2.5) | 0.73 (3) | 2.56 |
| LDM | 0.50 (4) | 0.50 (4) | 0.53 (4) | 0.50 (4) | 0.57 (4) | 0.58 (4) | 0.50 (4) | 0.59(4) | 4.00 |
| LDM+ Composite LGM | 0.74 (2) | **0.96 (1.5)** | 0.80 (2.5) | 0.81 (3) | 0.80 (2) | 0.92 (2) | 0.75 (2.5) | 0.75 (2) | 2.19 |
| Point Series | **0.96 (1)** | 0.95 (3) | **0.90 (1)** | **0.95 (1)** | **0.97 (1)** | **0.95 (1)** | **0.92 (1)** | **0.91 (1)** | **1.25** |
| | $\sum_{j=1}^{k} \mu_j^2 = 28.91$ | | | | | | | | |
| | Friedman test statistic = 18.77 (*p-value* = 0.009) | | | | | | | | |
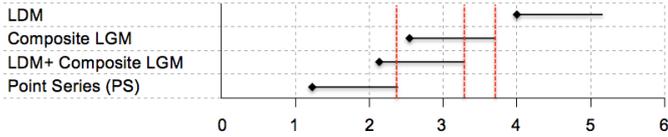


Figure 14: The average rank ($\mu_i$) associated with CD value for the classifiers generated using same data sets.
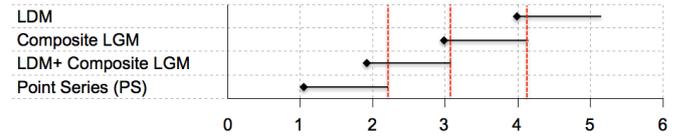


Figure 15: The average rank ($\mu_i$) associated with CD value for the classifiers generated using different data sets.

presents the average AUC values obtained in each case. The calculated Friedman statistic with its associated *p-value* (as shown in the table) strongly confirmed again that the PS technique produces the best performance according to its average ranking. Again we can also observe that there is a significant statistical difference between the operation of PS and both the LDM and Composite LGM techniques. In summary, when considering the AUC performance measures, it can be concluded that PS technique yields the best performance while the LDM technique performs significantly worse than the other proposed techniques. However, the operation of two *individual* classification techniques (in some cases) yielded classification performances whose differences are not statistically significant such as in the case of (i) Composite LGM and the combined LDM + Composite LGM, (ii) PS and the combined LDM + Composite LGM and (iii) LDM and Composite LGM as shown in Figure 15.

## 8. Conclusion

This paper has presented three different techniques (LGM, LDM and PS) to represent 3D surfaces for the purpose of building classifiers to predict a phenomena known as "springback". The novelty of the proposed techniques is their ability to capture the na-

ture of the local geometries associated with the 3D surfaces of interest. A Springback Prediction Framework was also proposed to generate springback predictors (classifiers) and to apply them. The LGM technique represented the points on a 3D surface using a concept similar to local binary patterns. The LDM technique represented the points in terms of their proximity to the nearest critical feature (edges). The PS technique represented the surface in terms of spiral linearisation curves. Two flat-topped pyramid shapes (Gonzalo and Modified) were used for evaluation purposes.

The main findings were as follows:

- The proposed techniques could be effectively used to represent 3D surfaces in a format suited to classifier generation.

- The PS technique outperforms the other techniques in terms of both AUC and accuracy, some excellent results were obtained.

- The application of the Friedman test demonstrated that the operation of the classifiers generated (with the same data set), using the composite LGM and the LDM techniques, was statistically different from the operation of the classifiers generated using the PS or the LDM + composite LGM techniques.

Table 21: The best AUC results for the proposed techniques (variations) with respect to each 3D representation technique using different data set to train and test the classifier.

| | GS1 | GS2 | GT1 | GT2 | MS1 | MS2 | MT1 | MT2 | $\mu_i$ |
|---|---|---|---|---|---|---|---|---|---|
| Composite LGM | 0.70 (3) | 0.74 (3) | 0.75 (3) | 0.81 (3) | 0.82 (3) | 0.80 (3) | 0.76 (3) | 0.76 (3) | 3.00 |
| LDM | 0.52 (4) | 0.50 (4) | 0.61 (4) | 0.50 (4) | 0.60 (4) | 0.60 (4) | 0.50 (4) | 0.60(4) | 4.00 |
| LDM+ Composite LGM | 0.94 (2) | 0.90 (2) | 0.89 (2) | 0.97 (2) | 0.92 (2) | 0.95 (1.5) | 0.93 (2) | 0.86 (2) | 1.94 |
| Point Series | **0.99 (1)** | **1.00 (1)** | **0.99 (1)** | **1.00 (1)** | **1.00 (1)** | 0.95 (1.5) | **1.00 (1)** | **0.99 (1)** | **1.06** |
| | $\sum_{j=1}^{k} \mu_j^2$ = 29.88 <br> Friedman test statistic = 23.42 (*p-value* = 0.001) | | | | | | | | |

- Similarly the application of the Friedman test demonstrated that there is *no significant* difference between the PS and the combined LDM + composite LGM technique (using either the same/different data set), although the PS technique produced some very good results.

Overall these were very encouraging results indicating that the proposed techniques, especially the PS technique, could be effectively used for springback prediction and consequent mitigation with respect to sheet metal forming processes such as AISF. For future work the research team intend to investigate mechanisms to propose corrections to the input cloud for a given shape so as to produced a corrected input cloud $C_{corr}$ in order to compensate for the springback introduced during manufacturing in the context of processes such as AISF process. This will also require a suitable format for the $C_{corr}$ cloud to facilitate manufacturing. The authors are also interested in producing an "intelligent process model" where the $C_{corr}$ cloud is iteratively refined until the predicted shape (generated from $C_{corr}$ using classification processes of the form described in this paper) is equivalent to $C_{in}$ (the desired shape).

## 9. Acknowledgement

## References

Abramowitz, M., & I.A. Stegun, I. (1964). *Handbook of Mathematical Functions: With Formulars, Graphs, and Mathematical Tables.* Applied mathematics series. New York : Dover Publications.

Adams, D. (2013). A highly-effective Incremental/Decremental Delaunay Mesh-Generation Strategy for Image Representation. *Signal Process.*, *93*, 749–764.

Alexa, M., Behr, J., Cohen, D., Fleishman, S., Levin, D., & Silva, C. (2001). Point Set Surfaces. In *Proceedings of the conference on Visualization '01* VIS '01 (pp. 21–28). Washington, DC, USA: IEEE Computer Society.

Ayache, N. (1995). Medical computer vision, virtual reality and robotics. *Image and Vision Computing*, *13*, 295 – 313.

Behera, A. K., Verbert, J., Lauwers, B., & Duflou, J. (2013). Tool Path Compensation Strategies for Single Point Incremental Sheet Forming using Multivariate Adaptive Regression Splines. *Computer-Aided Design*, *45*, 575 – 590.

Berger, H., Klein, M., & Mller, T. (2011). Deformation and vibration measurement and data evaluation on large structures employing optical measurement techniques. In T. Proulx (Ed.), *Rotating Machinery, Structural Health Monitoring, Shock and Vibration, Volume 5* Conference Proceedings of the Society for Experimental Mechanics Series (pp. 547–554). Springer New York.

Biasotti, S., Giorgi, D., Spagnuolo, M., & Falcidieno, B. (2008). Reeb Graphs for Shape Analysis and Applications. *Theoretical Computer Science*, *392*, 5 – 22.

Breiman, L., Friedman, J., Stone, C., & Olshen, R. (1984). *Classification and Regression Trees.* (1st ed.). Chapman and Hall/CRC.

BS ISO 1101 (2005). BS ISO 1101:2005 Geometrical Product Specifications (GPS) - Geometrical tolerancing - Tolerances of form, orientation, location and run-out- Generalities, definitions, symbols, indications on drawings.

Cafuta, G., Mole, N., & Łtok, B. (2012). An enhanced displacement adjustment method: Springback and thinning compensation. *Materials and Design*, *40*, 476 – 487.

Chatti, S. (2010). Effect of the Elasticity Formulation in Finite Strain on Springback Prediction. *Computers and Structures*, *88*, 796 – 805.

Chatti, S., & Hermi, N. (2011). The Effect of Non-linear Recovery on Springback Prediction. *Computers and Structures*, *89*, 1367 – 1377.

Dasarathy, B. (1991). *Nearest Neighbor (NN) Norms: NN Pattern Classification Techniques.* IEEE Computer Society Press tutorial. IEEE Computer Society Press.

Demoly, F., Toussaint, L., Eynard, B., Kiritsis, D., & Gomes, S. (2011). Geometric Skeleton Computation Enabling Concurrent Product Engineering and Assembly Sequence Planning. *Computer-Aided Design*, *43*, 1654 – 1673.

Demšar, J. (2006). Statistical comparisons of classifiers over multiple data sets. *J. Mach. Learn. Res.*, *7*, 1–30.

El-Salhi, S., Coenen, F., Dixon, C., & Khan, M. (2012). Identification of correlations between 3d surfaces using data mining techniques: Predicting springback in sheet metal forming. In M. Bramer, & M. Petridis (Eds.), *Research and Development in Intelligent Systems XXIX* (pp. 391–404). Springer London.

Farin, G., Hoschek, J., & Kim, M. (2002). *Handbook of Computer Aided Geometric Design [electronic resource]*. Elsevier Science & Technology.

Firat, M., Kaftanoglu, B., & Eser, O. (2008). Sheet Metal Forming Analyses With An Emphasis On the Springback Deformation. *Journal of Materials Processing Technology*, *196*, 135 – 148.

Fisher, R., & Yates, F. (1970). *Statistical Tables for Biological,Agricultural,and Medical Research: 6th Ed Rev and Enl*. Hafoor.

Fresno, M., Vnere, M., & Clausse, A. (2009). A combined region growing and deformable model method for extraction of closed surfaces in 3d {CT} and {MRI} scans. *Computerized Medical Imaging and Graphics*, *33*, 369 – 376.

Friedman, M. (1940). A Comparison of Alternative Tests of Significance for the Problem of m Rankings. *The Annals of Mathematical Statistics*, *11*, 86–92.

Fu, Z., Mo, J., Chen, L., & Chen, W. (2010). Using Genetic Algorithm-Back Propagation Neural Network Prediction and Finite-Element Model Simulation to Optimize the Process of Multiple-Step Incremental Air-Bending Forming of Sheet Metal. *Materials and Design*, *31*, 267 – 277.

García, S., Fernández, A., Luengo, J., & Herrera, F. (2009a). A study of statistical techniques and performance measures for genetics-based machine learning: Accuracy and interpretability. *Soft Comput.*, *13*, 959–977.

García, S., Molina, D., Lozano, M., & Herrera, F. (2009b). A study on the use of non-parametric tests for analysing the evolutionary algorithms' behaviour: A case study on the cec'2005 special session on real parameter optimisation. *Journal of Heuristics*, *15*, 617–644.

Ghanei, A., Soltanian-Zadeh, H., & Windham, J. (1998). A 3d deformable surface model for segmentation of objects from volumetric data in medical images. *Computers in Biology and Medicine*, *28*, 239 – 253.

Goldfeather, J., Hultquist, J. P., & Fuchs, H. (1986). Fast Constructive-Solid Geometry Display in the Pixel-Powers Graphics System. *SIGGRAPH Comput. Graph.*, *20*, 107–116.

Guo, Z., Zhang, L., & Zhang, D. (2010). A Completed Modeling of Local Binary Pattern Operator for Texture Classification. *IEEE Transactions on Image Processing*, *19*, 1657–1663.

GW, B. (1983). Errors, types i and ii. *American Journal of Diseases of Children*, *137*, 586–591.

Han, J. (2005). *Data Mining: Concepts and Techniques*. San Francisco, CA, USA: Morgan Kaufmann Publishers Inc.

Hao, W., & Duncan, S. (2011). Optimization of Tool Trajectory for Incremental Sheet Forming Using Closed Loop Control. In *Automation Science and Engineering (CASE), 2011 IEEE Conference on* (pp. 779 –784).

Hoppe, H., DeRose, T., Duchamp, T., McDonald, J., & Stuetzle, W. (1992). Surface reconstruction from unorganized points. *SIGGRAPH Comput. Graph.*, *26*, 71–78.

Hsiao, S., & Chen, R. (2013). A study of surface reconstruction for 3d mannequins based on feature curves. *Computer-Aided Design*, .

Hubeli, A., & Gross, M. (2000). *A survey of Surface Representations for Geometric Modeling*. Technical Report.

Izquierdo, E., & Ohm, J. (2000). Image-based rendering and 3d modeling: A complete framework. *Signal Processing: Image Communication*, *15*, 817 – 858.

Jahanshahi, M., & Masri, S. (2012). Adaptive vision-based crack detection using 3d scene reconstruction for condition assessment of structures. *Automation in Construction*, *22*, 567 – 576.

Jain, R., Kasturi, R., & B.G.Schunck (1995). *Machine Vision*. McGraw-Hill series in computer science. McGraw-Hill.

Jeswiet, J., Micari, F., Hirt, G., Bramley, A., Duflou, J., & Allwood, J. (2005). Asymmetric Single Point Incremental Forming of Sheet Metal. *CIRP Annals - Manufacturing Technology*, *54*, 88 – 114.

Johnson, N., Kotz, S., & Balakrishnan, N. (1995). *Continuous univariate distributions*. Number v. 2 in Wiley series in probability and mathematical statistics: Applied probability and statistics. Wiley & Sons.

Keogh, E. J., & Pazzani, M. J. (2001). Derivative Dynamic Time Warping. In *In SIAM International Conference on Data Mining*.

Khan, M., Coenen, F., Dixon, C., & El-Salhi, S. (2012). Finding Correlations Between 3-d Surfaces: A study in Asymmetric Incremental Sheet Forming. In *Proc. Machine Learning and Data Mining in Pattern Recognition (MLDM'12), Springer LNAI 7376* (pp. 336–379).

Liu, W., Liang, Z., Huang, T., Chen, Y., & Lian, J. (2008). Process Optimal Ccontrol of Sheet Metal Forming Springback Based on Evolutionary Strategy. In *Intelligent Control and Automation, 2008. WCICA 2008. 7th World Congress on* (pp. 7940 –7945).

Liu, W., Liu, Q., Ruan, F., Liang, Z., & Qiu, H. (2007). Springback Prediction for Sheet Metal Forming Based on GA-ANN Technology. *Journal of Materials Processing Technology*, *187-188*, 227 – 231.

Lu, G., & Sajjanhar, A. (1999). Region-based Shape Representation and Similarity Measure Suitable for Content-based Image Retrieval. *Multimedia Syst.*, *7*, 165–174.

Munkberg, J., Hasselgren, J., Totht, R., & Akenine-Möller, T. (2010). Efficient Bounding of Displaced Bèzier Patches. In *Proceedings of the Conference on High Performance Graphics* HPG '10 (pp. 153–162). Aire-la-Ville, Switzerland,

21

Switzerland: Eurographics Association.

Narasimhan, N., & Lovell, M. (1999). Predicting Springback in Sheet Metal Forming: An Explicit to Implicit Sequential Solution Procedure. *Finite Elements in Analysis and Design*, *33*, 29 – 42.

Nasrollahi, V., & Arezoo, B. (2012). Prediction of Springback in Sheet Metal Components With Holes on the Bending Area, Using Experiments, Finite Element and Neural Networks. *Materials and Design*, *36*, 331 – 336.

Nemenyi, P. (1963). *Distribution-free multiple comparisons*. Ph.D. thesis New Jersey, USA.

Pinto, T., Kohler, C., & Albertazzi, A. (2012). Regular Mesh Measurement of Large Free Form Surfaces Using Stereo Vision and Fringe Projection. *Optics and Lasers in Engineering*, *50*, 910 – 916.

Quinlan, J. (1986). Induction of Decision Trees. *Machine Learning*, *1*, 81–106.

Quinlan, R. (1993). *C4.5: Programs for Machine Learning*. San Mateo, CA: Morgan Kaufmann Publishers.

Roth, G., & Wibowoo, E. (1997). An Efficient Volumetric Method for Building Closed Triangular Meshes from 3D Image and Point Data. In *In Graphics Interface 97* (pp. 173–180).

Sakoe, H., & Chiba, S. (1990). Readings in speech recognition. chapter Dynamic Programming Algorithm Optimization for Spoken Word Recognition. (pp. 159–165). San Francisco, CA, USA: Morgan Kaufmann Publishers Inc.

Song, I., & Yang, J. (2011). A scene Graph Based Visualization Method for Representing Continuous Simulation Data. *Computers in Industry*, *62*, 301 – 310.

Soucy, M., & Laurendeau, D. (1995). A general surface approach to the integration of a set of range views. *Pattern Analysis and Machine Intelligence, IEEE Transactions on*, *17*, 344–358.

Strano, M. (2005). Technological representation of forming limits for negative incremental forming of thin aluminum sheets. *Journal of Manufacturing Processes*, *7*, 122 – 129.

Tan, P., Steinbach, M., & Kumar, V. (2005). *Introduction to Data Mining, (First Edition)*. Boston, MA, USA: Addison-Wesley Longman Publishing Co., Inc.

Tisza, M. (2004). Numerical Modelling and Simulation in Sheet Metal Forming. *Journal of Materials Processing Technology*, *151*, 58 – 62.

Tsumoto, S. (2009). Contingency matrix theory: Statistical dependence in a contingency table. *Information Sciences*, *179*, 1615 – 1627.

Wei, L., & Keogh, E. (2006). Semi-supervised time series classification. In *Proceedings of the 12th ACM SIGKDD international conference on Knowledge discovery and data mining* KDD '06 (pp. 748–753). New York, NY, USA: ACM.

Wettschereck, D. (1994). *A study of Distance-based Machine Learning Algorithms*. Ph.D. thesis Corvallis, OR, USA.

Wu, X., Kumar, V., Quinlan, J. R., Ghosh, J., Yang, Q., Motodai, H., McLachlan, G., Ng, A., Liu, B., Yu, P., Zhou, Z., Steinbach, M., Hand, D., & Steinberg, D. (2007). Top 10 Algorithms in Data Mining. *Knowl. Inf. Syst.*, *14*, 1–37.

Xi, X., Keogh, E., Shelton, C., Wei, L., & Ratanamahatana, C. (2006). Fast time series classification using numerosity reduction. In *Proceedings of the 23rd international conference on Machine learning* ICML '06 (pp. 1033–1040). New York, NY, USA: ACM.

Yoon, J., Pourboghrat, F., Chung, K., & Yang, D. (2002). Springback Prediction For Sheet Metal Forming Process Using a 3D Hybrid Membrane/Shell Method. *International Journal of Mechanical Sciences*, *44*, 2133 – 2153.